waste

MDPI

Article

Polyolefin-Based Cladding Panels from Discarded Fishing Ropes: A Sustainable Solution for Managing Fishing Gear Waste in Isolated Islands

Zakariae Belmokhtar [1,*], Simon Sanchez-Diaz [1], Patrice Cousin [1], Saïd Elkoun [2] and Mathieu Robert [1]

[1] Departement of Civil Engineering, Université de Sherbrooke, 2500, Boulevard de l'Université, Sherbrooke, QC J1K2R1, Canada; simon.sanchez.diaz@usherbrooke.ca (S.S.-D.); patrice.cousin@usherbrooke.ca (P.C.); mathieu.robert2@usherbrooke.ca (M.R.)

[2] Department of Mechanical Engineering, Université de Sherbrooke, 2500, Boulevard de l'Université, Sherbrooke, QC J1K 2R1, Canada; said.elkoun@usherbrooke.ca

* Correspondence: zakariae.belmokhtar@usherbrooke.ca; Tel.: +1-819-580-8073

Abstract: This study investigates the potential for recycling fishing rope waste from the Magdalen Islands, Canada, into sustainable wall cladding panels, addressing both environmental concerns and waste management challenges. A comprehensive characterization of the fishing ropes was conducted using various analytical techniques to assess their suitability for recycling. Fourier transform infrared spectroscopy (FTIR) and X-ray diffraction (XRD) identified polyethylene (PE) and isotactic polypropylene (iPP) as the main polymers present in the ropes, with a composition of approximately 25% PE and 75% PP. The effects of photodegradation were evaluated through carbonyl index analysis, differential scanning calorimetry (DSC), tensile testing, and gel permeation chromatography (GPC). The results showed reduced crystallinity, a 20% decrease in tensile strength, and lower molecular weights due to environmental exposure in comparison with unused ropes. However, melt flow rate (MFR) measurements aligned with virgin HDPE and PP values used in rope manufacturing, indicating suitable processability for recycling. Panels produced from recycled fishing ropes exhibited lower flexural and impact properties compared to commercial alternatives due to the presence of mineral contaminants and voids in the panels as revealed by X-ray diffraction (XRD) and scanning electron microscopy (SEM). This comprehensive investigation provides valuable insights into the potential repurposing of fishing rope waste, contributing to the development of sustainable waste management strategies for coastal communities.

Keywords: high-density polyethylene; polypropylene; photodegradation; crystallinity

Citation: Belmokhtar, Z.; Sanchez-Diaz, S.; Cousin, P.; Elkoun, S.; Robert, M. Polyolefin-Based Cladding Panels from Discarded Fishing Ropes: A Sustainable Solution for Managing Fishing Gear Waste in Isolated Islands. *Waste* **2024**, *2*, 337–353. https://doi.org/10.3390/waste2030019

Academic Editor: Catherine N. Mulligan

Received: 27 May 2024
Revised: 12 August 2024
Accepted: 13 August 2024
Published: 16 August 2024

1. Introduction

Among all the anthropogenic environmental impacts, the generation and disposal of plastic waste has become one of the primary problems that current and future generations must address. It is estimated that more than half of the annual production of solid plastic, over 200 million tons, ends up being disposed in landfills or dumped in unsanitary dumpsites and water bodies [1]. Of this plastic waste, between 19 and 23 million tons are dumped into seas or open waters each year without any pre-treatment or sorting, and this number is projected to triple by 2040 [2].

Globally, an estimated 640,000 tons of fishing gear end up in the ocean each year [3], contributing significantly to marine pollution. This type of waste is called abandoned, lost, or otherwise discarded fishing gear (ALDFG). In a study conducted by Lebreton et al. [4], the authors predicted that out of 79,000 tons of plastic waste observed in the North Pacific Gyre, 46% corresponded to fishing-related debris. The main issue with this type of waste involves what is denominated ghost fishing, meaning that this litter continues to cause the death of aquatic species even when they are no longer actively used by fishermen. In a

2009 study, 870 ghost nets retrieved from the coasts of Washington contained the remains of more than 32,000 marine animals, 500 birds, and 23 mammals [5].

Photodegradation is the primary mechanism for plastic degradation in aquatic environments, consisting of three steps [6]. The first step, initiation, involves the breaking of chemical bonds in the polymer chain by light, generating free radicals. This process requires the presence of unsaturated chromophoric groups in the polymers, which absorb light energy [7]. While polypropylene (PP) and polyethylene (PE) theoretically resist photoinitiation due to the absence of unsaturated double bonds in their polymer backbones, small amounts of external impurities, such as stabilizers, can enable this initiation [8]. During the propagation step, polymer radicals react with oxygen, forming hydroperoxides [9,10]. This reaction leads to either chain scission or crosslinking [11]. Finally, the termination step is when inert products are formed from the combination of two radicals [6,12]. For PE and PP, these products include hydroxyl, carbonyl and vinyl groups [13–15]. PP exhibits lower photodegradation resistance compared to PE due to the presence of tertiary carbons in its molecular chain, which are more sensitive to oxygen attack [16,17]. The degradation process generally leads to a reduction in the molecular weight of the polymer, making the material more susceptible to fragmentation [18]. This leads to the generation of microplastics, which can move easily through the food chain and can lead to serious health problems [19].

Islands are particularly sensitive to the problem of accumulation of plastic waste due to the limitations in technology and size at their waste treatment facilities. For instance, the Magdalen Islands in Quebec, Canada, are a small archipelago in the Gulf of Saint Lawrence whose primary economic activities are fishing and tourism. Tons of fishing gear waste, including ropes, nets, buoys, lobster traps, cages, and other residues, are produced every year and exported to the Saint-Rosaire landfill in Quebec, approximately 1200 km away from the island. This transportation costs around $125 per ton and generates around 159 kg of CO_2 per trip [20]

Several initiatives have been put in place to recycle fishing waste, particularly fishing lines and ropes, to transform them into consumer products such as carpets, sunglasses, and skateboards [21–23]. Fishing nets have also been utilized as reinforcement in cement-based matrices [24,25]. However, the recycling of this type of waste is complicated because it usually consists of blends of various polymers, especially polyethylene, polypropylene, and nylon. In addition, this waste may contain organic debris that requires a costly cleaning process [26]. Despite these efforts, there is a lack of research on the feasibility of recycling photodegraded fishing ropes into construction products, a gap this study aims to address. The use of used fishing ropes for panel production represents a sustainable and cost-effective option for walls and ceilings. Such products may be versatile enough for a range of applications and environments, including production plants, commercial spaces, or governmental buildings.

This study aims to investigate the feasibility of recycling fishing ropes into wall panels, addressing both environmental concerns and waste management challenges in coastal regions. A comprehensive characterization of the fishing ropes was conducted by analyzing the molecular and mechanical properties of the used material, followed by a comparison of the flexural and impact properties of panels made from the used ropes with those of standard commercial vertical cladding panels. The results indicate that although the used rope panels have lower mechanical properties, they present a viable and environmentally friendly alternative for vertical wall cladding applications due to low photodegradation-induced chain scission and optimal processability.

2. Materials and Methods

2.1. Materials

Used fishing ropes and new fishing ropes were obtained from the Magdalen Islands, Canada from the CERMIM (Centre de Recherche sur les Milieux Insulaires et Maritimes). The used fishing ropes were collected from the waste management center after being discarded by fishermen at the end of their lifespan, which is estimated to be two to three

years. A sorting process was conducted to separate the polyolefin ropes from the nylon nets. This sorting was based on visual inspection, as nylon nets exhibited a smooth, polished texture, whereas polyolefin ropes had a rougher, less polished texture. For comparison, new fishing ropes were procured from Pro flex (Granby, QC, Canada). Both types of ropes were shredded separately on-site using a BM309 Pelletier Granulator (Granby, QC, Canada) without prior washing before processing. The resulting shredded ropes had an average size of 4 cm.

To enhance the uniformity of the ropes' properties, the shredded ropes underwent an initial extrusion cycle, where the resulting filament was converted into 2 mm pellets (Figure 1). These pellets were subsequently extruded a second time and fed into an injection molding machine. The two extrusion cycles and injection molding parameters are summarized in Table 1.

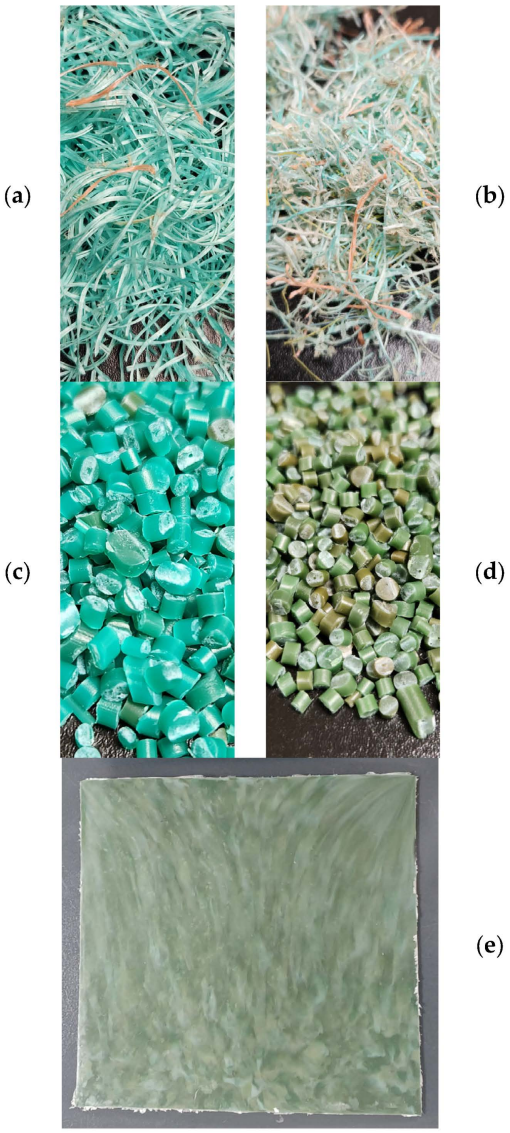

Figure 1. (**a**) Shredded new fishing ropes; (**b**) shredded used fishing ropes; (**c**) new fishing rope pellets; (**d**) used fishing rope pellets; (**e**) used fishing rope panel.

Table 1. Extrusion and injection molding parameters for fishing ropes.

Parameter	Value
Extruder used	Thermo Fischer Process 11 Twin-screw extruder (Waltham, MA, USA)
Extruder temperature zone	8 zones (Zone 1: 180 °C, Zones 2–8: 190 °C)
Die exit diameter	2 mm
Screw speed	70 RPM
Injection molding machine	HAAKE^{TM} MiniJet Pro (Waltham, MA, USA)
Molding time	10 s
Molding pressure	450 bars
Mold temperature	Room temperature

2.2. Manufacturing of Thin Films for Molecular Characterization

A 4533 AutoFour/3015-PL, H Carver press (Wabash, IN, USA) was used to produce thin films with a thickness of 15 µm. These films were made by placing 5 g of pellets between two aluminum films and then placing them in the press. The samples were compressed at a temperature of 200 °C and a pressure of 10 tons for two minutes. These samples were used to analyze the chemical composition and crystalline structure of the polymers present in the ropes.

2.3. Panel Manufacturing Process

Panels made from used fishing ropes were produced using the press 4533 AutoFour/3015-PL, H Carver (Wabash, IN, USA) (Figure 1e). First, 126 g of used fishing rope pellets were evenly distributed on the surface of a 200 mm × 200 mm × 3 mm metallic mold and compressed at 200 °C under a pressure of 8 tons for 10 min, followed by a cooling step at 30 °C under the same pressure for 8 min.

2.4. Characterization Techniques

The characterization techniques employed in this study included Fourier transform infrared spectroscopy (FTIR), differential scanning calorimetry (DSC), gel permeation chromatography (GPC), X-ray diffraction (XRD), melt flow rate (MFR), tensile testing, flexural testing, and the Notched Izod impact test. Each technique was applied to five samples, with the exceptions of GPC and XRD, which were analyzed using only two samples. Fourier transform infrared spectroscopy (FTIR) and X-ray diffraction (XRD) were performed on thin films, tensile testing was conducted on injection-molded samples, melt flow rate (MFR) and differential scanning calorimetry (DSC) tests were performed on pellets, and the remaining techniques were applied to the panels.

To determine if the difference between the average values of MFR, tensile, and DSC properties between the two types of ropes was statistically significant, a Welch's *t*-test was conducted at a 95% confidence level. Welch's *t*-test is an adaptation of Student's *t*-test designed for two samples that may have unequal variances [27]. The analysis included the mean, standard deviation, and *p*-value for each parameter. The *p*-value obtained from the test was compared to the significance level ($\alpha = 0.05$) to evaluate the null hypothesis that there is no difference in the mean value of each parameter between the two types of ropes.

2.4.1. Fourier Transform Infrared Spectroscopy (FTIR)

The chemical groups of polymers present in the ropes were determined using a Jasco FT/IR-4600, (Easton, MD, USA). For each spectrum, 32 scans were recorded at a resolution of 4 cm^{-1} from 4000 to 400 cm^{-1}.

The carbonyl index is a commonly used method for quantifying the photodegradation of polymer. The carbonyl index (**CI**) was calculated using Equation (1) [28]:

$$\mathbf{CI} = A_{(1850-1650)}/A_{(1500-1420)} \quad (1)$$

$\boldsymbol{A}$**(1850–1650)** is the integrated band absorbance of the carbonyl (C=O) peak from 1850 to 1650 cm^{-1} and $\boldsymbol{A}$**(1500–1420)** is that of the methylene (CH2) scissoring peak from 1500 to 1420 cm^{-1} [28]. This technique was used on the two types of ropes.

2.4.2. Differential Scanning Calorimetry (DSC)

This technique was used to determine the crystallization and melting temperatures, as well as the degree of crystallization of polymers present in the ropes. Samples weighing 15 mg were analyzed using a DSC Q2000 TA Instruments (Newcastle, DE, USA). The samples underwent a thermal cycle consisting of an initial heating from 0 °C to 200 °C, followed by an isothermal step of 1 min. Subsequently, the samples were cooled down to 0 °C and then reheated to 200 °C and recooled to 0 °C using a heating and cooling ramp of 10 °C/min. The first heating and cooling cycles were conducted to erase the thermal history of the samples.

Estimating the percentages of polymers in ropes is important, as these percentages are linked to the characteristics of the material and enable crystallinity levels to be evaluated. The percentages of polypropylene (PP) and polyethylene (PE) in the ropes were estimated using a calibration curve developed by Larsen et al. [29]. Various used PP–PE blends were produced, and the enthalpy of PE in these blends was presented as a function of the percentage of PE in the mixtures. This relationship is described by the following equation:

$$\mathbf{\%PE = 0.753 \times \Delta H_{PE} + 2.69} \quad (2)$$

where $\mathbf{\Delta H_{PE}}$ is the melting enthalpy of PE and %PE is the percentage of PE in the blend.

The degree of crystallinity (**Xc**) of the polymers was calculated using Equation (3):

$$\mathbf{Xc}\ (\%) = \frac{\boldsymbol{\Delta Hfi}}{\boldsymbol{\Delta H0 \cdot wi}} \times \mathbf{100} \quad (3)$$

In this equation, $\boldsymbol{\Delta Hfi}$ is the melting enthalpy of PP or PE, and $\boldsymbol{\Delta H0}$ corresponds to the melting enthalpy of a completely crystalline material, 205 J/g for polypropylene and 293 J/g for polyethylene, respectively [30], and $\boldsymbol{wi}$ stands for the weight of the polymer fraction in the rope. This technique was used on the two types of ropes.

2.4.3. Tensile Tests

Injection-molded specimens were used to study the impact of photodegradation on the tensile strength and Young's modulus of the panels. The tensile testing was carried out following ISO 527-2 guidelines [31], using a Zwich/Roell Z050 (Ulm, Baden-Württemberg, Germany) universal testing machine. During the tests, the samples were submitted to a constant load of 2 mm/min at a temperature of 25 °C, and the strain–stress data of the samples was recorded until breaking point. The dimensions of the specimen in mm are presented in Figure 2. This technique was performed on the two types of ropes.

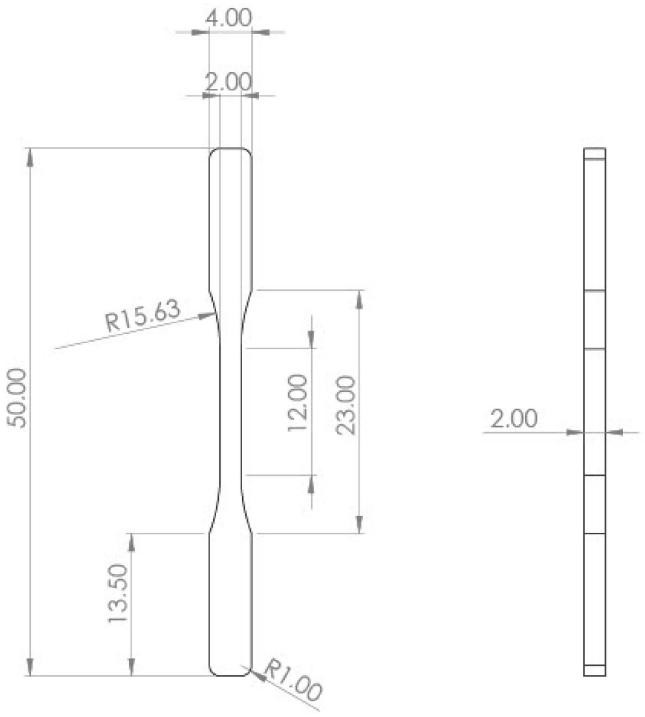

Figure 2. Tensile sample dimensions according to ISO 527-2 [31].

2.4.4. Gel Permeation Chromatography (GPC)

Gel permeation chromatography (GPC) was employed to study polymer chain scission of ropes due to photodegradation. An Agilent 1260 Infinity II HT (Santa Clara, CA, USA) GPC system was used for these analyses, using 1,2,4-trichlorobenzene (1,2,4-TCB) with 0.025% butylated hydroxytoluene (BHT) as the eluent. BHT is used for stabilization, as it removes free radicals that could produce organic peroxides [32]. Both 1,2,4-TCB and BHT had purities exceeding 99% and were obtained from Sigma-Aldrich (St. Louis, MO, USA).

The samples were dissolved overnight at a temperature of 160 °C and were analyzed the following day at a constant flow rate of 1 mL/min. Detection was conducted using a refractive index detector, and the chosen columns were 3 xPLgel Mixed-B (7.5 × 300 mm, 10 µm). Conventional calibration was conducted using six polystyrenes with molecular weights ranging from 580 to 67,600 g/mol on 2701 data points for each sample. This technique was performed on the two types of ropes. For each sample, the number-averaged molecular weight (Mn), weight-averaged molecular weight (Mw), and polydispersity index (PI = Mw/Mn) were measured.

2.4.5. Melt Flow Rate (MFR)

The melt flow rate (MFR) is calculated by heating the polymer to a specified temperature and extruding it through a die under a prescribed load. The MFR is then calculated as the mass of polymer extruded per unit time, typically expressed in grams per 10 min (g/10 min). For our study, the MFR tests were conducted using a Lab-Integration plastometer (Sherbrooke, QC, Canada) in accordance with the ASTM D1238-23 standard [33] at 230 °C with a 2.16 kg weight.

This technique provides insights into the material's behavior during melt-processing operations [34,35]. It also serves as an indicator of molecular changes caused by environmental exposure and recycling and is influenced by two competing processes that occur during environmental degradation: chain scission and crosslinking. Chain scission, which results in a reduction in molecular weight, typically leads to an increase in MFR due to enhanced polymer chain mobility. Conversely, crosslinking, which increases molecular weight through the formation of bonds between polymer chains, generally causes a decrease in MFR [36,37].

2.4.6. X-ray Diffraction (XRD)

X-ray diffraction (XRD) was used to examine the crystalline structure of polymer ropes and identify potential contaminants. The samples were analyzed using an X'Pert Pro MPD X-Ray diffractometer (Malvern, Worcestershire, UK) with an angle (2θ) range from 15° to −40°, and a step size of 0.04 degrees. The divergent slit was adjusted to 0.5 degrees, and the anti-scatter slit was set to 1 degree.

2.4.7. Flexural Tests

The flexural properties of the panels were assessed using a using a Zwick/Roell Z050 (Haan, Germany) universal testing machine in accordance with the ASTM D790-17 standard [38]. Five rectangular samples were cut from the panels, each measuring 80 mm in length, 12.7 mm in width, and 3 mm in thickness with a span of 48 mm. The flexural properties were measured using a crosshead speed of 1.2 mm/min.

2.4.8. Notched Izod Impact Tests

Notched Izod impact tests were conducted using an Instron CEAST-9050 (Norwood, MA, USA) machine with a 1 J pendulum, following the guidelines of the ASTM D256-23 standard [39]. The samples are 64 mm long, 12.7 mm wide, and 3 mm thick.

2.4.9. Scanning Electron Microscopy (SEM)

The microstructure of the specimen from the flexural testing was analyzed using a JEOL's NeoScope JCM-7000 (Easton, MD, USA) benchtop scanning electron microscope. Images of the microstructure were captured at a landing voltage of 15 kV and a magnification of 350×.

3. Results

3.1. FTIR

Figure 3 displays the FTIR spectrum of the two types of ropes. The peaks at 718 cm^{-1} (-CH2- rock), 729 cm^{-1} (split -CH2- rocking vibration), 2848 cm^{-1} (-CH2- symmetric stretch), 2914 and 2954 cm^{-1} (-CH2- asymmetric stretch), and 1377 cm^{-1} (-CH3- umbrella bending mode) correspond to the characteristic signal of polyethylene [40]. Meanwhile, the peaks at 840 cm^{-1} (C-CH3 stretching vibration), 997 and 1165 cm^{-1} (-CH3- rocking vibration), 1375 cm^{-1} (symmetric bending vibration of -CH3), 2952 cm^{-1} (-CH3 asymmetric stretching vibration), and 1455, 2838, and 2917 cm^{-1} (-CH2- symmetric bending, -CH2- symmetric stretching, and -CH2- asymmetric stretching) are typical isotactic polypropylene peaks [41,42]. The peak at 1255 cm^{-1} may be attributed to the presence of small amounts of polyvinyl chloride [43]. This was not expected but could be due to PVC-coated wire lobster trap debris in the ropes [44].

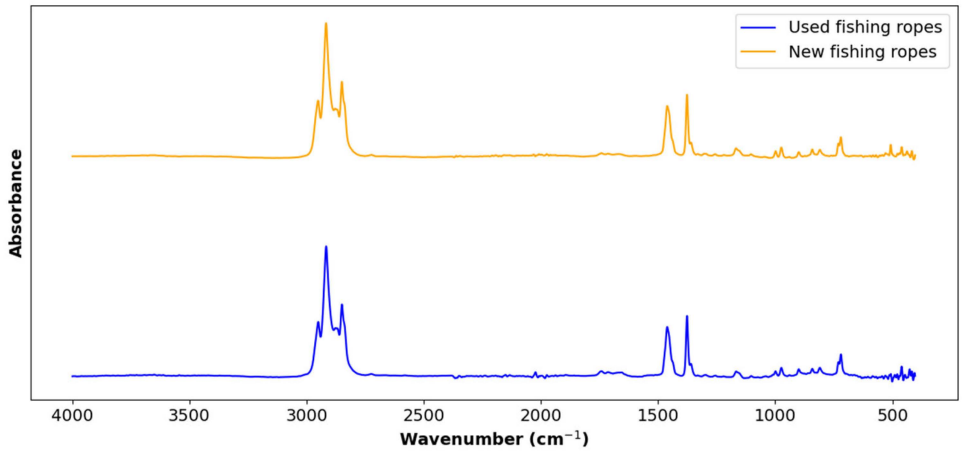

Figure 3. Fourier transform infrared spectra of used ropes vs. new ropes.

Table 2 presents the values of CI for the used and new fishing ropes. The used ropes showed a carbonyl index higher than that of new fishing ropes. This difference can be attributed to the photodegradation of old fishing ropes caused by prolonged exposure to sunlight and UV radiation. Martinez-Romo et al. [45] observed that HDPE exhibits an increase of 20% of the carbonyl index after 60 days of exposure to UV-B radiation.

Table 2. Carbonyl index (%) of used and new fishing ropes.

Sample	CI
Used fishing ropes	0.66
New fishing ropes	0.25

3.2. DSC

Figure 4 displays the DSC curves of the two types of ropes. Using Equation (2), it was determined that approximately 25% of both the used and new fishing ropes consisted of PE, while the remaining 75% was PP. Nevertheless, it is important to note that this estimation applied specifically to the batch of fishing ropes used in this study, considering the wide range of fishing ropes available in the market. Further studies are needed to explore the variability of rope composition and its potential influence on other the properties of the ropes.

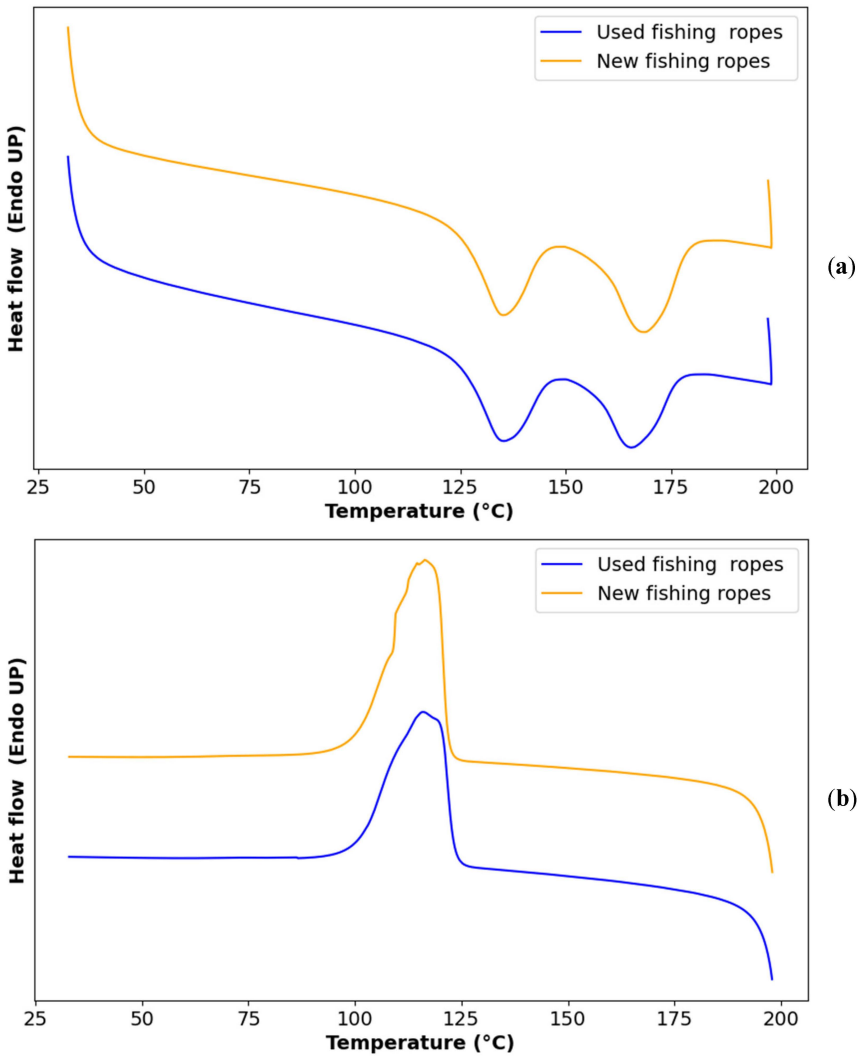

Figure 4. (**a**) Melting DSC curve of used vs. new ropes; (**b**) crystallization DSC curve of used vs. new ropes.

The melting and crystallization temperatures, as well as the enthalpies of both used and new fishing ropes, are presented in Table 3. The melting peak around 135 °C was closer to the one of HDPE than that of LDPE. In addition, the second melting peak corresponds to the characteristic melting behavior of isotactic polypropylene (iPP) which typically melts at temperatures ranging from 160 °C to 170 °C [46,47].

Table 3. Melting temperature (Tm), crystallization temperature (Tc), and degree of crystallinity (Xci) for polyethylene (1) and polypropylene (2) for new and used ropes.

		Used Fishing Ropes	New Fishing Ropes
Tc (°C)	Mean	117.24	116.1
	Standard deviation	0.1	0.24
	p-value	2×10^{-3}	
Tm1 (°C)	Mean	166.46	169.22
	Standard deviation	0.23	0.21
	p-value	5×10^{-8}	
Xc1 (%)	Mean	18.08	19.3
	Standard deviation	0.64	0.67
	p-value	0.02	
Tm2 (°C)	Mean	135.18	135.2
	Standard deviation	0.15	0.1
	p-value	0.56	
Xc2 (%)	Mean	42.56	45.28
	Standard deviation	1.64	1.57
	p-value	0.02	

Figure 4a shows a single crystallization peak, corresponding to the overlapping crystallization events of the two main polymers, HDPE and iPP, due to their close crystallization temperatures and the faster crystallization kinetics of HDPE compared with iPP [48].

Upon comparing the melting and crystallization behavior of new and used ropes (Table 3), it was observed that the melting temperature of PP shifted lower, with a *p*-value of 5×10^{-8}. This *p*-value indicates that the null hypothesis, which states there is no difference in the melting temperature of PP between new and used ropes, can be rejected as it is lower than 0.05. The significant difference might have arisen from the possible chain scission caused by photodegradation, which might lead to a decrease in molecular weight and a subsequent drop in the melting temperature of the polymer. However, the melting temperature of PE remained unchanged, as indicated by a *p*-value of 0.56. This can be attributed to the differential impact of photodegradation between PP and PE.

The used ropes exhibited significantly lower degrees of crystallinity for both PP and PE compared to new ropes ($p = 0.02$ for both Xc1 and Xc2). This reduction could be attributed to a disruption in the crystalline structure of the polymers, possibly caused by the formation of crosslinks that hinder crystallization, or by the accumulation of oxidation products that disrupt the orderly arrangement of polymer chains [49]. This result is in contrast with some studies suggesting that chain scission increases the mobility of polymer chains, facilitating their crystallization and consequently leading to a higher degree of crystallinity [50,51].

The degrees of crystallinity of polyethylene and polypropylene in the ropes are lower than those of pure HDPE and PP found in the literature [48,52–54], which may be attributed to their low degree of miscibility. This phenomenon could influence the formation and density of spherulites, resulting in the decreased crystallinity of the two polymers [55].

The polymers in the used ropes presented acceptable degrees of crystallinity, as they are higher than the ones found by Stewart et al. [56], who reported degrees of crystallinity

of 10.71% and 25.96% for virgin HDPE and PP, respectively, in a 25% HDPE and 75% PP blend.

3.3. Tensile Tests

Figure 5 illustrates the stress–strain curves of injection-molded samples from both new and used ropes.

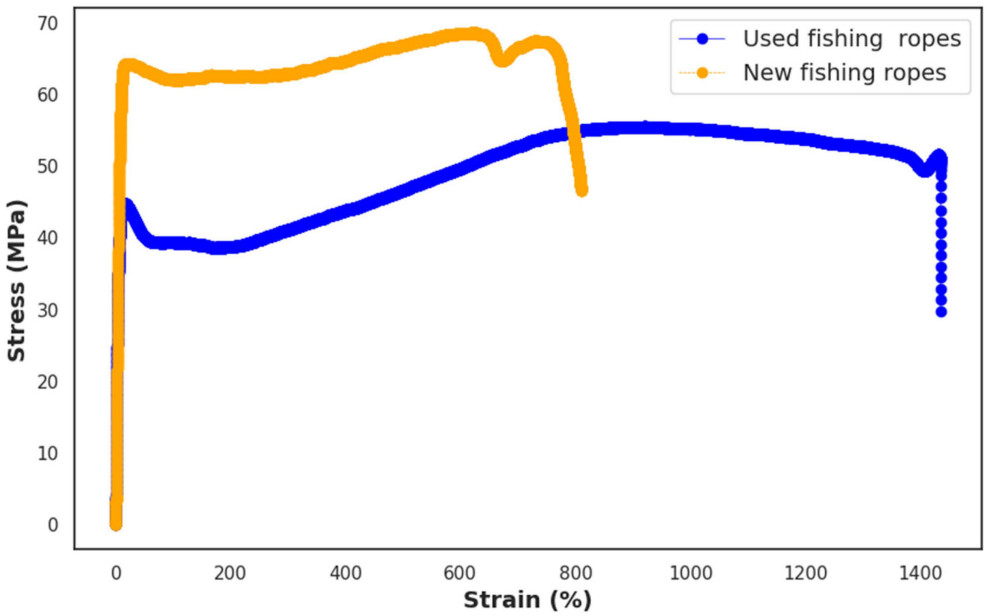

Figure 5. Stress–strain curves for the used and new fishing ropes.

Table 4 presents the tensile properties of new and used fishing ropes. It can be observed that the *p*-value for the modulus of elasticity was greater than 0.05, indicating that the null hypothesis is not rejected. This implies that there was no statistically significant difference between the modulus of elasticity of the new and used ropes, which is consistent with the results reported by Jones et al. [57], who also reported a small difference between the elastic modulus of virgin and used HDPE–PP blends.

Table 4. Tensile properties of used and new fishing ropes.

		Used Fishing Ropes	**New Fishing Ropes**
Young's modulus (Gpa)	Mean	1.31	1.31
	Standard deviation	0.16	0.024
	p-value	0.99	
Tensile strength (Mpa)	Mean	54.2	68.4
	Standard deviation	3.21	3.51
	p-value	10^{-4}	
Elongation at break (%)	Mean	1425	810
	Standard deviation	83.89	52.08
	p-value	3.47×10^{-6}	

For the tensile strength and elongation at break, the difference between the two types of ropes was statistically significant, as the *p*-value was lower than 0.05. The loss of 20% of the tensile strength of the used ropes could be attributed to a reduction in the molecular weight of the polymer, which consequently resulted in a reduction in tensile strength. This loss was not significant for the application purpose, as wall panels are not typically subjected

to significant tensile loads. The tensile strength of steel-fiber-reinforced concrete panels is reported to be around 6.2 MPa, which is only 5% of its compressive strength [58]. Used roped exhibited a higher elongation at break when compared to the sample made of new ropes. The increase in elongation of the used polymer could be attributed to the enhanced flexibility of the polymer chains resulting from chain scission due to photodegradation [59].

3.4. GPC

Table 5 presents the results for number-averaged molecular weight (Mn), weight-averaged molecular weight (Mw), and polydispersity index (PD index) of new and used fishing ropes, obtained via gel permeation chromatography (GPC). These results indicate that the used ropes experienced a 12% reduction in number-averaged molecular weight (Mn) and a 10% decrease in weight-averaged molecular weight (Mw). This reduction can be attributed to polymer chain scission resulting from photo-oxidation. However, an increase in the PD index was also observed, suggesting the occurrence of crosslinking alongside chain scission [60], likely due to the composite nature of the ropes, with HDPE prone to crosslinking while PP predominantly undergoes chain scission [61].

Table 5. Molecular weights and polydispersity index (PI) of new and used ropes.

Rope Type	Number Average (Mn) in g/mol	Weight Average (Mw) in g/mol	Polydispersity Index (PI)
New fishing ropes	90,227	409,615	4.53
Used fishing ropes	79,032	368,203	4.65

The reduction in molecular weight appears to have a more significant impact on the tensile strength than on the modulus. This may be attributed to the occurrence of crosslinking in parallel with chain scission, which resulted in an increase in the stiffness of the polymer, and as the molecular mass decreased beyond a certain point, the stiffness returned to its initial value. This phenomenon was observed by Becerra et al. [48] in their study on the UV degradation of HDPE, where they found that Young's modulus increased by 35% after eight weeks of UV exposure before it began to decline. An alternative hypothesis is that the crosslinking and molecular mass reduction were not sufficiently significant to cause a notable change in the rigidity of the polymer. This is supported by a study modeling the degradation process of semi-crystalline polymers, which found that Young's modulus declined only after a significant number of chain scissions have occurred [62].

3.5. MFR

Table 6 compares the melt flow rate (MFR) of new and used fishing ropes. The used ropes showed a significantly higher MFR, increasing by 35% ($p < 0.05$). Gel permeation chromatography (GPC) indicated chain scission through a reduced molecular weight, while the polydispersity index suggested some crosslinking. The overall MFR increase demonstrates that chain scission was the primary degradation mechanism, despite potentially concurrent processes.

Table 6. MFR of the used and new ropes.

		New Fishing Ropes	Used Fishing Ropes
MFR (g/10 min)	Mean	1.35	1.82
	Standard deviation	0.2	0.11
	p-value	0.02	

The melt flow rate of polymers used in rope manufacturing falls within the following ranges: 0.9 to 3 g/10 min for HDPE [63–65] and 1.8 to 3 g/10 min for PP [66,67]. The MFR

of the used ropes is within the acceptable range, aligning with the values observed for commercial virgin PP and HDPE used in rope manufacturing. This indicates that the used fishing ropes retained suitable flow properties for processing and could be incorporated into existing manufacturing processes to produce new products, such as the wall cladding panels presented in this study, as MFR is an indicator of the flowability and processability of thermoplastic polymers [34,35].

3.6. XRD

Polypropylene has three crystal structures including the α-phase, the β-phase, and the γ-phase. The α-phase is the most stable and common structure [68]. In a crystallography diagram, the α-phase appears as five distinct peaks observed at 2θ angles of 14.2°, 17.1°, 18.88°, 21.2°, and 21.94° [69].

The metastable β-phase is induced by nucleating agents and is characterized by a chiral crystal structure with complex chain orientation [68]. In a crystallography diagram, the β-phase appears as a single peak at an angle 2θ equal to 16.2°. The presence of β-crystals improves polypropylene's toughness and fire resistance but reduces its modulus of elasticity [70–73].

Figure 6 presents the crystallography diagram of the sample made from used fishing ropes. This plot showed the five characteristic peaks of PP α-crystals. Additionally, two characteristic peaks of HDPE were observed in the plot. The first one occurred at 21.7°and appeared as a large peak overlapping with the peaks of PP α-crystals at 21.2° and 21.9°. The second HDPE peak appeared as a single signal at 24.1° [74]. No β-crystals were present for the PP in the ropes due to the absence of a β-crystalline peak at 2θ = 16.2° [75]. α-PP is more susceptible to UV degradation than β-PP. In a study conducted by Obadal et al. [75], the cracking patterns of α-PP and β-PP were examined after long-term exposure to UV light. The authors found that α-PP displayed deep, distant cracks, while β-PP exhibited a dense network of fine cracks that were only visible under a microscope. The absence of β-crystals for the used ropes may be a factor contributing to the photodegradation of PP.

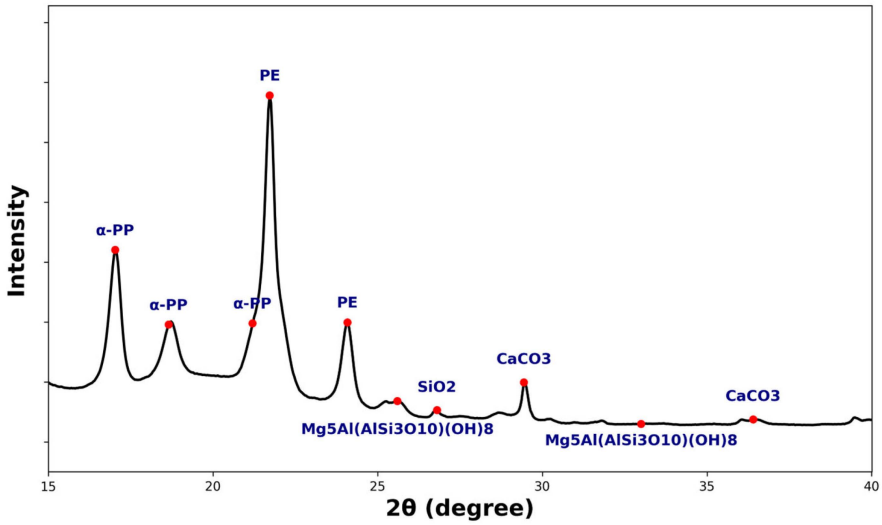

Figure 6. X-ray diffraction pattern for the used fishing ropes.

The other peaks corresponded to signals from pollutants such as calcite ($CaCO_3$), quartz (SiO_2), or clinochlore ($Mg_5Al\ (Si_3Al)O_{10}\ (OH)_8$), resulting from the contact between the ropes and either seashells or sand [76].

3.7. Flexural and Notched Izod Impact Strength Test

Table 7 shows a comparison between the flexural and impact properties of the panels made from used fishing ropes and commercially available cladding panels. Commercial panels were also tested in accordance with ASTM D790 for flexural properties and ASTM

D256 for Izod impact properties. The properties of the commercial panels, as displayed in Table 7, were sourced from the manufacturer's technical data sheet, and were not measured by the authors.

The panels made of fishing ropes exhibited inferior flexural modulus and impact strength compared to the commercially available panels. This difference can be primarily attributed to the fact that the fishing rope panel is composed of a blend of PP and HDPE, which are immiscible polymers, resulting in poor mechanical properties when blended. Lin et al. [77] demonstrated that blending PP with HDPE at a 75%/25% ratio resulted in a 12.7% decrease in flexural strength and a 36.4% decrease in flexural modulus in comparison with pure PP. In another study, the impact strength of a 50% PP/50% HDPE blend was found to be 50% lower than that of pure PP [78]. Additionally, the commercial panels are made from virgin polymers, whereas the fishing rope panel is made from used polymers. Other contributing factors include the presence of mineral impurities in the ropes, as revealed by XRD analysis, and the presence of voids in the panels panel, as shown in Figure 7, which all act as crack initiation points, ultimately leading to a decrease in the mechanical properties [79].

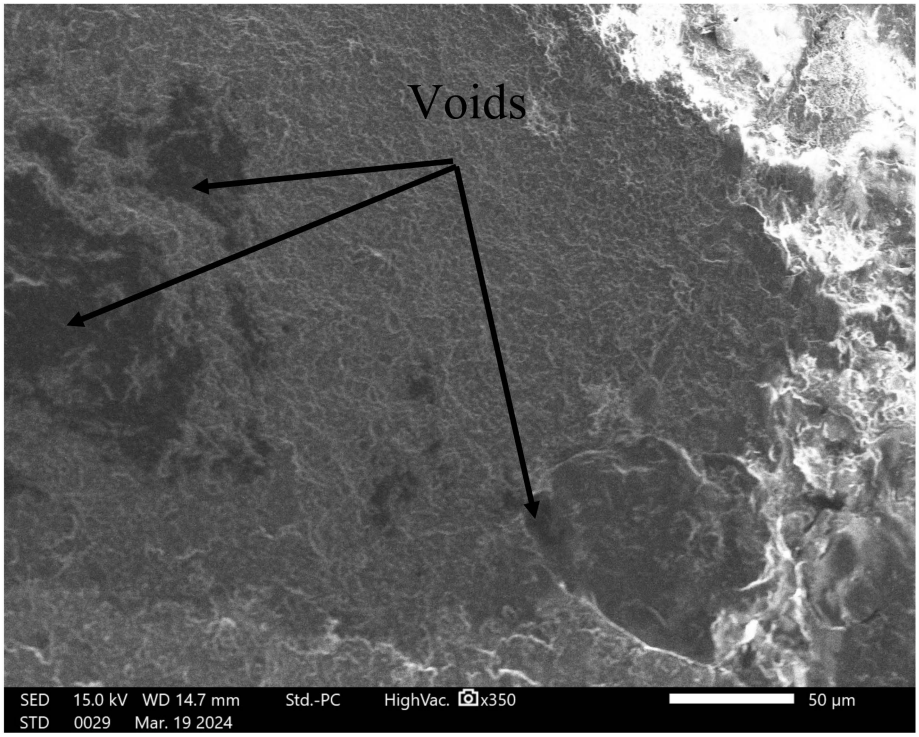

Figure 7. Scanning electron microscope image of the fishing rope panel.

Table 7. Flexural and Izod impact properties comparison of used ropes and commercial wall cladding panels.

Panel Type/Manufacturer	Material	Flexural Strength (Mpa)	Flexural Modulus (Gpa)	Izod Impact Strength (J/m)	Source
Used fishing rope panel	PP-HDPE	10	0.23	30.73	----
MULFORD Plastics	HDPE	----	1.379	159	[80]
CPS	HDPE	----	----	374	[81]
SIMONA	HDPE	---	1.65	147	[82]

While wall cladding panels generally experience low stress during use, they may face significant loads during transportation and installation. Therefore, improving the mechanical properties of used panels is crucial for their practical application. Optimizing

the manufacturing process could improve the properties of the used fishing rope panels. This optimization can be achieved through methods such as applying cyclic loading to reduce the presence of air bubbles in the panels, or by adding natural fibers or inorganic powders, which studies suggest leads to an improvement in mechanical properties [83–86].

4. Conclusions

This study demonstrates the feasibility of recycling fishing ropes into cladding panels, with a comprehensive analysis of their molecular and mechanical properties. FTIR and DSC analyses confirmed the presence of PE and iPP in the fishing ropes, while also revealing evidence of photodegradation. Tensile tests and GPC analyses indicated polymer chain degradation and decreased molecular weight, resulting in reduced tensile strength compared to virgin materials. However, MFR measurements showed that the used ropes retained suitable flow properties for processing, despite the occurrence of chain scission. XRD analysis revealed only α-phase crystalline peaks for PP in the ropes. However, the detection of mineral contaminants points to the potential need for additional purification steps in the recycling process.

Despite the inferior flexural and impact properties of the used panels compared to commercial counterparts, this study establishes a foundation for future research on the valorization of fishing gear waste. The production of wall panels from used fishing ropes demonstrates the potential for creating value-added products from marine plastic waste, supporting waste management strategies in remote island communities and providing a sustainable solution to marine plastic pollution.

Future research should focus on enhancing the mechanical properties of the panels through the incorporation of reinforcing agents or compatibilizers. Additionally, exploring different processing techniques, such as blending with virgin polymers or employing advanced extrusion and molding technologies, could further optimize the properties of the used panels. The approach developed in this study could potentially be adapted for other types of fishing gear, such as nylon nets.

Author Contributions: Z.B. conceptualized the study, defined the methodology, collected and analyzed the data, and wrote the manuscript. S.S.-D., M.R., P.C. and S.E. were involved in editing and reviewing the manuscript and provided funding for the research study. All authors have read and agreed to the published version of the manuscript.

Funding: Research was funded by MITACS, grant number IT39206.

Institutional Review Board Statement: Not applicable.

Informed Consent Statement: Not applicable.

Data Availability Statement: The original contributions of this study are included in the article. For further information, please contact the corresponding author.

Acknowledgments: The authors thank the Centre de Recherche sur les Milieux Insulaires et Maritimes (CERMIM) for providing the materials used in this study.

Conflicts of Interest: The authors declare no conflicts of interest.

References

1. Ritchie, H.; Samborska, V.; Roser, M. "Plastic Pollution". 2023. Published Online at OurWorldInData.org. Available online: https://ourworldindata.org/plastic-pollution (accessed on 21 May 2024).
2. United Nations Environment Programme. "Plastic Pollution". 2023. Published Online at UNEP.org. Available online: https://www.unep.org/plastic-pollution (accessed on 1 January 2024).
3. Greenpeace, "Ghost Gear: The Abandoned Fishing Nets Haunting Our Oceans", Greenpeace. 2019. Available online: https://www.greenpeace.org/static/planet4-international-stateless/2019/11/8f290a4f-ghostgearfishingreport2019_greenpeace.pdf (accessed on 17 May 2023).
4. Lebreton, L.; Slat, B.; Ferrari, F.; Sainte-Rose, B.; Aitken, J.; Marthouse, R.; Hajbane, S.; Cunsolo, S.; Schwarz, A.; Levivier, A.; et al. Evidence that the Great Pacific Garbage Patch is rapidly accumulating plastic. *Sci. Rep.* **2018**, *8*, 4666. [CrossRef]

5. Good, T.P.; June, J.A.; Etnier, M.A.; Broadhurst, G. *Ghosts of the Salish Sea: Threats to Marine Birds in Puget Sound and the Northwest Straits from Derelict Fishing Gear*; NOAA Fisheries/National Marine Fisheries Service, Conservation Biology Division, Northwest Fisheries Science Center: Seattle, WA, USA, 2009.
6. Pritchard, G. *Plastics Additives*; Springer: Dordrecht, The Netherlands, 1998; Volume 1.
7. Gijsman, P.; Meijers, G.; Vitarelli, G. Comparison of the UV-degradation chemistry of polypropylene, polyethylene, polyamide 6 and polybutylene terephthalate. *Polym. Degrad. Stab.* **1999**, *65*, 433–441. [CrossRef]
8. Norman, G.; Gerald, S. *Polymer Degradation & Stabilisation*; Cambridge University Press: Cambridge, UK; New York, NY, USA, 1988.
9. Singh, B.; Sharma, N. Mechanistic implications of plastic degradation. *Polym. Degrad. Stab.* **2008**, *93*, 561–584. [CrossRef]
10. Jan, F. *Rabek, Polymer Photodegradation*; Springer: Dordrecht, The Netherlands, 1995. [CrossRef]
11. Tolinski, M. *Additives for Polyolefins: Getting the Most Out of Polypropylene, Polyethylene and TPO*; William Andrew Pub: Oxford, UK, 2009.
12. Scott, G. (Ed.) *Degradable Polymers*; Springer: Dordrecht, The Netherlands, 2002. [CrossRef]
13. De Carvalho, C.L.; Silveira, A.F.; Rosa, D.D.S. A study of the controlled degradation of polypropylene containing pro-oxidant agents. *Springerplus* **2013**, *2*, 623. [CrossRef] [PubMed]
14. Doğan, M. Ultraviolet light accelerates the degradation of polyethylene plastics. *Microsc. Res. Tech.* **2021**, *84*, 2774–2783. [CrossRef]
15. Carrasco, F.; Pagès, P.; Pascual, S.; Colom, X. Artificial aging of high-density polyethylene by ultraviolet irradiation. *Eur. Polym. J.* **2001**, *37*, 1457–1464. [CrossRef]
16. Gewert, B.; Plassmann, M.M.; MacLeod, M. Pathways for degradation of plastic polymers floating in the marine environment. *Environ. Sci. Process Impacts* **2015**, *17*, 1513–1521. [CrossRef]
17. Weber, R.; Watson, A.; Forter, M.; Oliaei, F. Review Article: Persistent organic pollutants and landfills—A review of past experiences and future challenges. *Waste Manag. Res. J. A Sustain. Circ. Econ.* **2011**, *29*, 107–121. [CrossRef]
18. Summers, J.W.; Rabinovitch, E.B. *Weathering of Plastics*; Elsevier: Amsterdam, The Netherlands, 1999.
19. Marfella, R.; Prattichizzo, F.; Sardu, C.; Fulgenzi, G.; Graciotti, L.; Spadoni, T.; D'Onofrio, N.; Scisciola, L.; La Grotta, R.; Frigé, C.; et al. Microplastics and Nanoplastics in Atheromas and Cardiovascular Events. *N. Engl. J. Med.* **2024**, *390*, 900–910. [CrossRef]
20. CERMIM. "Rapport Projet de Valorisation des Cordages". Report Published Online at CERMIM.ca. 2023. Available online: https://www.cermim.ca/wp-content/uploads/2023/08/200129_Rapport-Projet-valorisation-Cordages_CERMIM-1-108.pdf (accessed on 12 February 2024).
21. Econyl. NET-WORKSTM. Available online: https://www.econyl.com/magazine/econyl-news/net-works/ (accessed on 21 May 2024).
22. Waterhaul. Recycled, Sustainable Sunglasses & Ocean Plastic Products. Available online: https://waterhaul.co/ (accessed on 21 May 2024).
23. Bureo. Bureo—Recycled Fishing Nets Products. Available online: https://bureo.co/ (accessed on 21 May 2024).
24. Park, J.K.; Kim, D.J.; Kim, M.O. Mechanical behavior of waste fishing net fiber-reinforced cementitious composites subjected to direct tension. *J. Build. Eng.* **2021**, *33*, 101622. [CrossRef]
25. Truong, V.D.; Kim, M.O.; Kim, D.J. Feasibility study on use of waste fishing nets as continuous reinforcements in cement-based matrix. *Constr. Build. Mater.* **2021**, *269*, 121314. [CrossRef]
26. European Commission. *Study on Circular Design of the Fishing Gear for Reduction of Environmental Impacts*; European Commission: Brussels, Belgium, 2020.
27. Ahad, N.A.; Yahaya, S.S.S. Sensitivity analysis of Welch's *t*-test. *AIP Conf. Proc.* **2014**, *1605*, 888–893. [CrossRef]
28. Almond, J.; Sugumaar, P.; Wenzel, M.N.; Hill, G.; Wallis, C. Determination of the carbonyl index of polyethylene and polypropylene using specified area under band methodology with ATR-FTIR spectroscopy. *E-Polymers* **2020**, *20*, 369–381. [CrossRef]
29. Larsen, Å.G.; Olafsen, K.; Alcock, B. Determining the PE fraction in recycled PP. *Polym. Test.* **2021**, *96*, 107058. [CrossRef]
30. TA Instruments. Thermal Conductivity (TN048). Available online: https://www.tainstruments.com/pdf/literature/TN048.pdf (accessed on 16 February 2024).
31. *ISO 527-2*; Plastics—Determination of Tensile Properties—Part 2: Test Conditions for Moulding and Extrusion. ISO: Geneva, Switzerland, 2012.
32. Bivens, A. "Step-by-Step Method Development for GPC/SEC". Published Online at Agilent Technologies, Inc. 2016. Available online: https://www.agilent.com/cs/library/technicaloverviews/public/5991-7272EN.pdf (accessed on 1 July 2024).
33. *ASTM D1238-23*; Standard Test Method for Melt Flow Rates of Thermoplastics by Extrusion Plastometer. ASTM: West Conshohocken, PA, USA, 2013.
34. Singh, R.; Kumar, R.; Ahuja, I.S. Thermal Analysis for Joining of Dissimilar Polymeric Materials Through Friction Stir Welding. In *Reference Module in Materials Science and Materials Engineering*; Elsevier: Amsterdam, The Netherlands, 2017. [CrossRef]
35. Bremner, T.; Rudin, A.; Cook, D.G. Melt flow index values and molecular weight distributions of commercial thermoplastics. *J. Appl. Polym. Sci.* **1990**, *41*, 1617–1627. [CrossRef]
36. Strömberg, E.; Karlsson, S. The design of a test protocol to model the degradation of polyolefins during recycling and service life. *J. Appl. Polym. Sci.* **2009**, *112*, 1835–1844. [CrossRef]
37. Oblak, P.; Gonzalez-Gutierrez, J.; Zupančič, B.; Aulova, A.; Emri, I. Processability and mechanical properties of extensively recycled high density polyethylene. *Polym. Degrad. Stab.* **2015**, *114*, 133–145. [CrossRef]

38. *ASTM D790-17*; Standard Test Methods for Flexural Properties of Unreinforced and Reinforced Plastics and Electrical Insulating Materials. ASTM: West Conshohocken, PA, USA, 2017.
39. *ASTM D256-23*; Standard Test Methods for Determining the Izod Pendulum Impact Resistance of Plastics. ASTM: West Conshohocken, PA, USA, 2023.
40. Smith, B.C. The Infrared Spectra of Polymers II: Polyethylene. *Spectroscopy* **2021**, *36*, 24–29. [CrossRef]
41. Karger-Kocsis, J. (Ed.) *Polypropylene*; Springer: Dordrecht, The Netherlands, 1999; Volume 2. [CrossRef]
42. Larkin, P.J. Illustrated IR and Raman Spectra Demonstrating Important Functional Groups. In *Infrared and Raman Spectroscopy*; Elsevier: Amsterdam, The Netherlands, 2018; pp. 153–210. [CrossRef]
43. Amar, H.; Chabira, S.; Sebaa, M.; Benchatti, A. Structural Changes Undergone During Thermal Aging and/or Processing of Unstabilized, Dry-blend and Rigid PVC, Investigated by FTIR-ATR and Curve Fitting. *Ann. Chim.-Sci. Matériaux* **2019**, *43*, 59–68. [CrossRef]
44. Laufer, H.; Baclaski, B.; Koehn, U. Alkylphenols affect lobster (*Homarus americanus*) larval survival, molting and metamorphosis. *Invertebr. Reprod. Dev.* **2012**, *56*, 66–71. [CrossRef]
45. Martínez-Romo, A.; González-Mota, R.; Soto-Bernal, J.J.; Rosales-Candelas, I. Investigating the degradability of HDPE, LDPE, PE-Bio, and pe-oxo films under UV-B radiation. *J. Spectrosc.* **2015**, *2015*, 1–6. [CrossRef]
46. Lu, H.; Qiao, J.; Xu, Y.; Yang, Y. Effect of isotacticity distribution on the crystallization and melting behavior of polypropylene. *J. Appl. Polym. Sci.* **2002**, *85*, 333–341. [CrossRef]
47. Wei, H.; Thompson, R.B.; Park, C.B.; Chen, P. Surface tension of high density polyethylene (HDPE) in supercritical nitrogen: Effect of polymer crystallization. *Colloids Surf. A Physicochem. Eng. Asp.* **2010**, *354*, 347–352. [CrossRef]
48. Aumnate, C.; Rudolph, N.; Sarmadi, M. Recycling of Polypropylene/Polyethylene Blends: Effect of Chain Structure on the Crystallization Behaviors. *Polymers* **2019**, *11*, 1456. [CrossRef]
49. Pracella, M.; Rolla, L.; Chionna, D.; Galeski, A. Compatibilization and properties of poly(ethylene terephthalate)/polyethylene blends based on recycled materials. *Macromol. Chem. Phys.* **2002**, *203*, 1473–1485. [CrossRef]
50. Jabarin, S.A.; Lofgren, E.A. Photooxidative effects on properties and structure of high-density polyethylene. *J. Appl. Polym. Sci.* **1994**, *53*, 411–423. [CrossRef]
51. Fabiyi, J.S.; McDonald, A.G. Degradation of polypropylene in naturally and artificially weathered plastic matrix composites. *Maderas. Cienc. Tecnol.* **2014**, *16*, 12. [CrossRef]
52. Parenteau, T.; Ausias, G.; Grohens, Y.; Pilvin, P. Structure, mechanical properties and modelling of polypropylene for different degrees of crystallinity. *Polymer* **2012**, *53*, 5873–5884. [CrossRef]
53. Tarani, E.; Arvanitidis, I.; Christofilos, D.; Bikiaris, D.N.; Chrissafis, K.; Vourlias, G. Calculation of the degree of crystallinity of HDPE/GNPs nanocomposites by using various experimental techniques: A comparative study. *J. Mater. Sci.* **2023**, *58*, 1621–1639. [CrossRef]
54. Batista, N.L.; Helal, E.; Kurusu, R.S.; Moghimian, N.; David, E.; Demarquette, N.R.; Hubert, P. Mass-produced graphene—HDPE nanocomposites: Thermal, rheological, electrical, and mechanical properties. *Polym. Eng. Sci.* **2019**, *59*, 675–682. [CrossRef]
55. Shanks, R.A.; Li, J.; Yu, L. Polypropylene–polyethylene blend morphology controlled by time–temperature–miscibility. *Polymer* **2000**, *41*, 2133–2139. [CrossRef]
56. Stewart, K.M.E.; Stonecipher, E.; Ning, H.; Pillay, S.B. Mixing rules for high density polyethylene-polypropylene blends. *Can. J. Chem. Eng.* **2023**, *101*, 5395–5407. [CrossRef]
57. Jones, H.; McClements, J.; Ray, D.; Hindle, C.S.; Kalloudis, M.; Koutsos, V. Thermomechanical Properties of Virgin and Recycled Polypropylene—High-Density Polyethylene Blends. *Polymers* **2023**, *15*, 4200. [CrossRef]
58. Graybeal, B.A. *Material Property Characterization of Ultra-High Performance Concrete*; Office of Infrastructure Research and Development: Washington, DC, USA, 2006.
59. Ali, M.M.; Abdullah, A.; Mohamad, E.; Salleh, M.S.; Hussein NI, S.; Muhammad, Z.; Dahaman, S. Tensile properties of ternary blends for HDPE/PP/RECYCLE HDPE in blow moulding process. *J. Adv. Manuf. Technol.* **2018**, *12*, 31–41.
60. Grause, G.; Chien, M.-F.; Inoue, C. Changes during the weathering of polyolefins. *Polym. Degrad. Stab.* **2020**, *181*, 109364. [CrossRef]
61. Shyichuk, A.V.; Stavychna, D.Y.; White, J.R. Effect of tensile stress on chain scission and crosslinking during photo-oxidation of polypropylene. *Polym. Degrad. Stab.* **2001**, *72*, 279–285. [CrossRef]
62. Ding, L.; Davidchack, R.L.; Pan, J. A molecular dynamics study of Young's modulus change of semi-crystalline polymers during degradation by chain scissions. *J. Mech. Behav. Biomed. Mater.* **2012**, *5*, 224–230. [CrossRef] [PubMed]
63. PolymerExport. HDPE 5000S Monofilament. Available online: https://polymerexport.com/product/hdpe-5000s-monofilament/ (accessed on 26 June 2024).
64. Haldia Petrochemicals. Technical Data Sheet HD T10S. Available online: https://www.haldiapetrochemicals.com/img/newPdf/TDS%20HD%20T10S%2004052022.pdf (accessed on 26 June 2024).
65. OPaL India. Technical Data Sheet R5410. Available online: https://opalindia.in/assets/pdf/HDPE/Technical-Data/R5410.pdf (accessed on 26 June 2024).
66. TotalEnergies. Polypropylene PPH 3060. Available online: https://plastore.it/cgi2018/file818/6842_pp%20omo%20total%20pph3060.pdf (accessed on 26 June 2024).

67. Product Catalogue Polypropylene Tipplen Tatren Slovnaft Certificates. 2018. Available online: www.molgroupchemicals.com (accessed on 26 June 2024).
68. Sowinski, P.; Piorkowska, E.; Boyer, S.A.E.; Haudin, J.-M.; Zapala, K. The role of nucleating agents in high-pressure-induced gamma crystallization in isotactic polypropylene. *Colloid Polym. Sci.* **2015**, *293*, 665–675. [CrossRef] [PubMed]
69. Świetlicki, M.; Chocyk, D.; Klepka, T.; Prószyński, A.; Kwaśniewska, A.; Borc, J.; Gładyszewski, G. The Structure and Mechanical Properties of the Surface Layer of Polypropylene Polymers with Talc Additions. *Materials* **2020**, *13*, 698. [CrossRef]
70. Varga, J. β-Modification of Isotactic Polypropylene: Preparation, Structure, Processing, Properties, and Application. *J. Macromol. Sci. Part B* **2002**, *41*, 1121–1171. [CrossRef]
71. Papageorgiou, D.G.; Bikiaris, D.N.; Chrissafis, K. Effect of crystalline structure of polypropylene random copolymers on mechanical properties and thermal degradation kinetics. *Thermochim. Acta* **2012**, *543*, 288–294. [CrossRef]
72. Papageorgiou, D.G.; Papageorgiou, G.Z.; Bikiaris, D.N.; Chrissafis, K. Crystallization and melting of propylene–ethylene random copolymers. Homogeneous nucleation and β-nucleating agents. *Eur. Polym. J.* **2013**, *49*, 1577–1590. [CrossRef]
73. Tordjeman, P.; Robert, C.; Marin, G.; Gerard, P. The effect of α, β crystalline structure on the mechanical properties of polypropylene. *Eur. Phys. J. E* **2001**, *4*, 459–465. [CrossRef]
74. Madhu, G.; Bhunia, H.; Bajpai, P.K.; Chaudhary, V. Mechanical and morphological properties of high density polyethylene and polylactide blends. *J. Polym. Eng.* **2014**, *34*, 813–821. [CrossRef]
75. Obadal, M.; Čermák, R.; Raab, M.; Verney, V.; Commereuc, S.; Fraïsse, F. Structure evolution of α- and β-polypropylenes upon UV irradiation: A multiscale comparison. *Polym. Degrad. Stab.* **2005**, *88*, 532–539. [CrossRef]
76. Saeed, A.; Adewuyi, S.O.; Ahmed, H.A.M.; Alharbi, S.R.; Al Garni, S.E.; Abolaban, F. Electrical and Dielectric Properties of the Natural Calcite and Quartz. *Silicon* **2022**, *14*, 5265–5276. [CrossRef]
77. Lin, J.-H.; Pan, Y.-J.; Liu, C.-F.; Huang, C.-L.; Hsieh, C.-T.; Chen, C.-K.; Lin, Z.-I.; Lou, C.-W. Preparation and Compatibility Evaluation of Polypropylene/High Density Polyethylene Polyblends. *Materials* **2015**, *8*, 8850–8859. [CrossRef] [PubMed]
78. Ramazani, S.A.A.; Valami, M.A.; Khak, M. Effect of Poly (Propylene-g-maleic Anhydride) on the Morphological, Rheological, and Mechanical Properties of PP/HDPE Blend. *J. Thermoplast. Compos. Mater.* **2009**, *22*, 519–530. [CrossRef]
79. Daramola, O.; Taiwo, A.; Oladele, I.; Olajide, J.; Adeleke, S.; Adewuyi, B.; Sadiku, E. Mechanical properties of high density polyethylene matrix composites reinforced with chitosan particles. *Mater. Today Proc.* **2021**, *38*, 682–687. [CrossRef]
80. Mulford Plastics. HDPE Leaflet. Available online: https://www.mulfordplastics.com.au/media/1257/hdpe-leaflet.pdf (accessed on 21 May 2024).
81. Creative Panel Solutions. Laminated HDPE Panels. Available online: https://bpi.build/webres/File/building_materials/cps/Laminated-Poly-Data-Page.pdf (accessed on 21 May 2024).
82. Simona America Industries. Simona® Hdpe Polytone® Sheet. Available online: https://www.simona-america.com/fileadmin/user_upload/USA/Applications/Outdoor/Playground/16_SIMONA-HDPE-Polytone.pdf (accessed on 21 May 2024).
83. Park, B.; Balatinecz, J.J. Mechanical properties of wood-fiber/toughened isotactic polypropylene composites. *Polym. Compos.* **1997**, *18*, 79–89. [CrossRef]
84. Wu, J.; Yu, D.; Chan, C.-M.; Kim, J.; Mai, Y.-W. Effect of fiber pretreatment condition on the interfacial strength and mechanical properties of wood fiber/PP composites. *J. Appl. Polym. Sci.* **2000**, *76*, 1000–1010. [CrossRef]
85. Huang, Z.; Lin, Z.; Cai, Z.; Mai, K. Physical and mechanical properties of nano-$CaCO_3$/PP composites modified with acrylic acid. *Plast. Rubber Compos.* **2004**, *33*, 343–352. [CrossRef]
86. Buasri, A.; Chaiyut, N.; Borvornchettanuwat, K.; Chantanachai, N.; Thonglor, K. Thermal and Mechanical Properties of Modified $CaCO_3$/PP Nanocomposites. *Int. J. Metall. Mater. Eng.* **2012**, *6*, 689–692.